https://doi.org/10.18321/ectj1516

Synthesis, Structure, and Energetic Characteristics of Perovskite Photocatalyst $SrTiO_3$: an Experimental and DFT Study

A.D. Kudaibergen[1], Zh.B. Kuspanov[1,2]*, A.N. Issadykov[2,3], R.E. Beisenov[4], Z.A. Mansurov[5], M.A. Yeleuov[1,2,5], Ch.B. Daulbayev[2,6]

[1]Satbayev University, 22a Satbayev str., Almaty, Kazakhstan
[2]Institute of Nuclear Physics, 1 Ibragimova str., Almaty, Kazakhstan
[3]Joint Institute for Nuclear Research, 6 Joliot-Curie str., Dubna, Moscow Region, Russia
[4]Kazakh-British Technical University, 59 Tole by Str., Almaty, Kazakhstan
[5]Institute of Combustion Problems, 172 Bogenbay Batyr str., Almaty, Kazakhstan
[6]National Laboratory Astana, Nazarbayev University, 53 Kabanbay Batyr Ave., Astana, Kazakhstan

Article info

Received:
8 April 2023

Received in revised form:
26 May 2023

Accepted:
14 June 2023

Keywords:
Photocatalysts, $SrTiO_3$, Precipitation method, DFT, Quantum ESPRESSO, PBE

Abstract

$SrTiO_3$-based photocatalysts have become widely used due to their excellent properties such as high thermal stability, photocorrosion resistance, and stable structure that can be modified by doping and making composites. In this work, $SrTiO_3$ powder was prepared from $Sr(NO_3)_2$ and TiO_2 precursors by a simple chemical precipitation method followed by calcination. It was determined that calcination at 900 °C followed by treatment in nitric acid solution produced cubic $SrTiO_3$ particles without the presence of any impurities. In addition, structural, morphology, and energetic characterization using experimental and theoretical aspects are presented. Within the framework of density functional theory, the electronic properties of $SrTiO_3$ have been investigated in the Quantum ESPRESSO software package using the PBE functional under the generalized gradient approximation (GGA). The band structure and density of states were obtained, and the width of the bandgap was determined.

1. Introduction

The transition to renewable energy sources is becoming an essential step in solving modern environmental problems and meeting the growing energy needs of society. Effective utilization of the most widespread and promising energy source – solar radiation is one of the most critical problems, for the solution of which the search for new materials with improved optical properties is underway. Among them semiconductor photocatalysts are of the greatest interest due to their good study and wide range of possible applications: water splitting for hydrogen production [1–3], CO_2 reduction [4, 5], water purification from pollutants [6–11], degradation of dyes [12, 13] and others. However, due to the presence of a wide bandgap, the optical spectrum of semiconductor photocatalysts is limited to the ultraviolet zone [1], which is 3–5% of the total energy of solar radiation [14]. For example, titanium dioxide, which is a well-studied material among photocatalysts, has a bandgap of 3.2 eV [14, 15]. In addition to the bandgap width, the critical parameters for photocatalysts are the low recombination rate of charge carriers and resistance to photocorrosion [16, 17]. To obtain materials with the required properties, doping is most often used as a method of modifying the crystal lattice of the photocatalyst by adding impurities.

*Corresponding author.
E-mail address: zhenis.kuspanov@gmail.com

The class of perovskites with the general formula ABO_3 has more photocatalytic active centers on the surface compared to conventional metal oxides [18] due to their crystal structure in which A cations are located in the center of the BO_3 octahedron. Among them, $SrTiO_3$ is considered one of the promising materials, whose attractiveness consists of its environmental friendliness, low cost, high thermal and chemical stability, and excellent resistance to photocorrosion [17–19]. The cubic structure of $SrTiO_3$ perovskite makes it possible to vary the composition of A and B nodes, to control the charge balance and by using various impurities such as Cr, Al, Pt, Ag, Rh, Mo, Fe, etc., it is possible to achieve an improvement in photocatalytic activity [16], since the doping or formation of heterostructure due to the replacement of A cations by cations with a different ionic radius reduces the band structure of the material [18]. Goto et al. [20] in 2018 conducted a study of the photocatalytic water splitting activity of $RhCrOx/SrTiO_3$:Al, they achieved an efficiency of converting solar energy into hydrogen energy (STH) of 0.4% using a panel photocatalytic reactor with an area of 1 m^2 in sunlight. This achievement demonstrates the prospects for using photocatalysts based on $SrTiO_3$ for large-scale photocatalytic water splitting. Recently, attention to the use of density functional theory (DFT) to calculate the electronic structure of many-particle systems in quantum physics and chemistry, in particular for modeling the properties of photocatalysts [14, 17, 18], has increased significantly.

Density functional theory (DFT), developed by Hohenberg and Cohn, is a method for calculating the electronic structure of molecules and condensed matter that is widely used in computational chemistry and physics [21]. This theory's essence is using electron density instead of the many-electron wave function in the Schrödinger equation to describe the electronic subsystem. The advantage of DFT over *ab initio* methods (e.g., the Hartree-Fock method) is higher accuracy and speed of calculations because, unlike the wave function, which depends on the three spatial coordinates of each of the N electrons (3N), the electron density is a function of only three spatial coordinates. However, DFT-based calculations cannot be applied in all cases because the exchange-correlation functionals responsible for approximating electron-electron interactions have limitations in accuracy due to the fact that no single functional can correctly describe all types of systems and interactions. Also, significant computational resources may be required to handle systems with a large number of atoms. Nevertheless, numerous studies show successful examples of the use of DFT computational methods [22–25]. Thus, it is obvious that the use of DFT calculations can help in finding and predicting the properties of new materials.

In this work, $SrTiO_3$ was synthesized, X-ray diffraction analysis, and EDX analysis were performed, and surface morphology was investigated by scanning electron microscopy (SEM) and transmission electron microscopy (TEM). To calculate the electronic properties of $SrTiO_3$, a model simulation of the crystal structure of $SrTiO_3$ was carried out using the Quantum-Espresso software code and applying the GGA-PBE exchange-correlation functional. The modeling results helped to evaluate the electronic properties of $SrTiO_3$, such as energy structure and bandgap width. The obtained results made it possible to better understand the behavior of the material and its potential applications as an efficient photocatalyst.

2. Experimental section

2.1. Photocatalyst preparation

To synthesize $SrTiO_3$ of high purity, a chemical precipitation method based on previous works was used [26–30]. $Sr(NO_3)_2$ (> 98% purity, Sigma Aldrich), TiO_2 (Sigma Aldrich, particle size: 0.27 μm, 0.35 μm, 0.48 μm) and $(COOH)_2*2H_2O$ (> 99.5%, Sigma Aldrich) were used as initial reagents. A concentrated 0.12 M solution of $Sr(NO_3)_2$ was prepared using distilled water. TiO_2 powder was then added in the ratio of Ti and Sr 1:1. The resulting suspension was treated for 30 min in an ultrasonic bath. After that, 0.4 M solution of $(COOH)_2*2H_2O$ was added dropwise with vigorous stirring. The pH of the resulting mixture was adjusted to 6–7 with 10% NH_3OH solution. The suspension was filtered, and the residue was washed several times with distilled water. The obtained powder was dried at 60 °C overnight and then calcined at 900 °C for 1 h. Figure 1 shows a schematic representation of the methodology for the synthesis of $SrTiO_3$ powder.

2.2. Photocatalyst characterization technique

The surface morphology of the samples was investigated using a scanning electron microscope (SEM) JEM-2100 (JEOL, Japan). Scanning transmission electron microscopy (STEM) TESCAN MAIA3 XMU was used to further study morphology in high resolution. XRD analysis was performed on a

Fig. 1. Schematic illustration of the process of $SrTiO_3$ synthesis by chemical precipitation method.

Drone-8 X-ray diffractometer with detection unit rotation angles ranging from 5° to 70° and a minimum step of 0.001°. The permissible deviation of the detection unit from the specified rotation angle was ±0.015°.

2.3. Computational study

Based on the density functional theory, the electronic structure of $SrTiO_3$ was investigated; the open-source Quantum ESPRESSO program package was used as a computer code. The cubic structure of $SrTiO_3$ shown in Fig. 2 belongs to the space group Pm3m at room temperature, the lattice constants (a = b = c) were co-valued to 3.905 Å [24]. The Perdew-Burke-Ernzerhof (PBE) functional was adopted for the exchange-correlation potential (XC) in the generalized gradient approximation (GGA). The ultra-soft pseudo potential (USPP) was applied to approximate the electron-nucleus interaction. A 6 × 6 × 6 × 6 k-point Monkhorst-Pack grid was used to integrate the Brillouin zone for the calculation of the self-consistent field, and a 20 × 20 × 20 × 20 grid for the inconsistent field. The electronic structure was determined for relaxed cells along the Γ-X-M-Γ-R-X [17] symmetry points in the Brillouin zone.

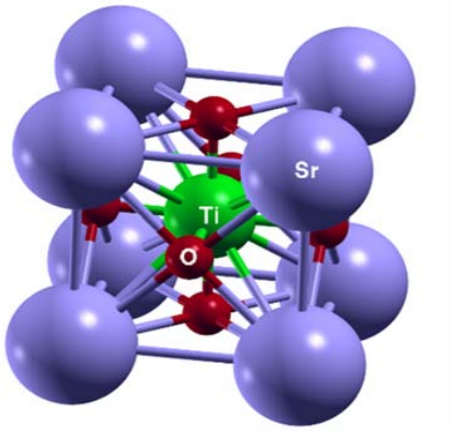

Fig. 2. Elementary cell of perovskite $SrTiO_3$.

3. Results and discussion

3.1. Photocatalyst characterization

The crystal structure of the semiconductor $SrTiO_3$ synthesized by chemical precipitation followed by calcination at 900 °C was studied by X-ray diffraction. Figure 3a shows typical diffraction peaks at 2θ equal to 32.23°, 39.98°, 46.50°, 57.83° and 67.64° corresponding to (110), (111), (200), (211), and (220) orientations of the $SrTiO_3$ crystal lattice. These peaks indicate that the semiconductor sample obtained via chemical precipitation is cubic $SrTiO_3$ and is consistent with standard data for $SrTiO_3$ (JCPDS Card No. 35-0734). It is particularly important to note that the peak at 2θ, equal to 32.23°, has a very high intensity, indicating that the semiconductor is highly crystalline. This is important because the transport efficiency of charged carriers arising from photogeneration can strongly depend on the crystallinity of the material. If the crystallinity is low, this can lead to inefficient migration of charged particles.

The choice of strontium titanate precursors with different sizes is due to the fact that, according to experimental data [31], when using smaller particles of TiO_2 precursors, the synthesis reaction is completed at lower temperatures and in less time, which indicates the dependence of the reaction rate on the surface area precursors. It was also established [31] that

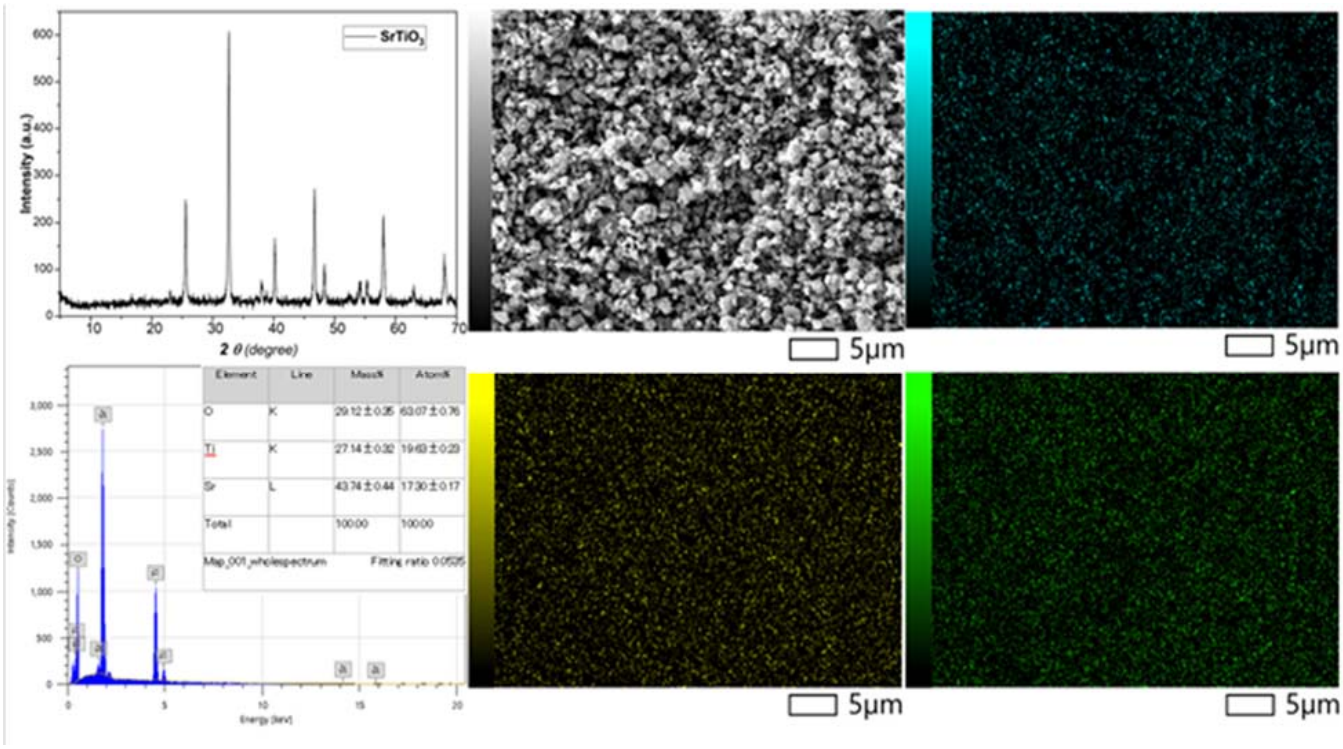

Fig. 3. X-ray spectra of synthesized $SrTiO_3$ powder – (a); energy dispersive X-ray spectrum of $SrTiO_3$ particles – (b); distributions of elements in the obtained sample by FIB-SEM method – (c-f).

the initial particle size of the TiO_2 precursor strongly affects the particle size of the reaction product obtained as a result of hydrothermal synthesis.

EDX analysis confirms the presence of O, Ti, and Sr in the obtained $SrTiO_3$ samples without any other impurities. Considering the atomic percentages of the synthesized sample as shown in Fig. 3d it can be found that Sr/Ti/O are 17.30%/19.63%/63.07%, respectively. In addition, the FIB-SEM technique was used to determine the distribution of elements in the obtained sample. Figure 3(c-f) shows the elemental maps for Sr, Ti and O in the $SrTiO_3$ sample. From the obtained maps, it can be seen that Sr, Ti, and O are uniformly distributed throughout the sample area.

The morphology of the obtained $SrTiO_3$ samples was studied by scanning (SEM) and transmission (TEM) electron microscope at different resolutions. As the results of scanning electron microscopy (Fig. 4) showed, we found that $SrTiO_3$ particles calcined at 900 °C have cubic shapes and sizes from 150 to 300 nm. Whereas increasing the calcination temperature to 1000 °C and 1100 °C increases the size of $SrTiO_3$ particles to the micrometer scale, which can negatively affect their photoactivity due to the increased distance that the photogenerated electrons and holes need to travel to the surface where the reactions occur. This increases the probability of recombination (charge fusion) and can reduce the efficiency of the reactions [30, 32]. Calcination at 800 °C leads to the formation of smaller particles but with more impurities such as $SrCO_3$ [33]. Based on literature and experimental data, the optimum calcination temperature is 900 °C followed by treatment in 1M nitric acid solution to remove residual $SrCO_3$. However, it should be noted that the particle sizes are very heterogeneous. From studies in the literature, it is clear that doping $SrTiO_3$ with other elements such as Al or Mn can contribute to the size reduction and distortion of the shape of $SrTiO_3$ crystals [34, 35].

In the case of TEM, one can see clearly formed cubes of $SrTiO_3$ with anisotropic structure, the average size of which is about 200 nm as can be seen from Fig. 5. An important feature of these particles is the anisotropic structure, which creates a difference in energy on different faces, leading to the formation of p-n junctions [36]. This allows the charge within each photocatalyst particle to be separated using an internal electric field. Thus, electrons are concentrated on some facets and holes on other facets, which helps to separate the photocatalytic reduction and oxidation processes on different facets [37]. Due to the anisotropic crystal structure, selective precipitation of co-catalysts occurs, which leads to the release of hydrogen and oxygen on the faces of the cubic photocatalyst [37].

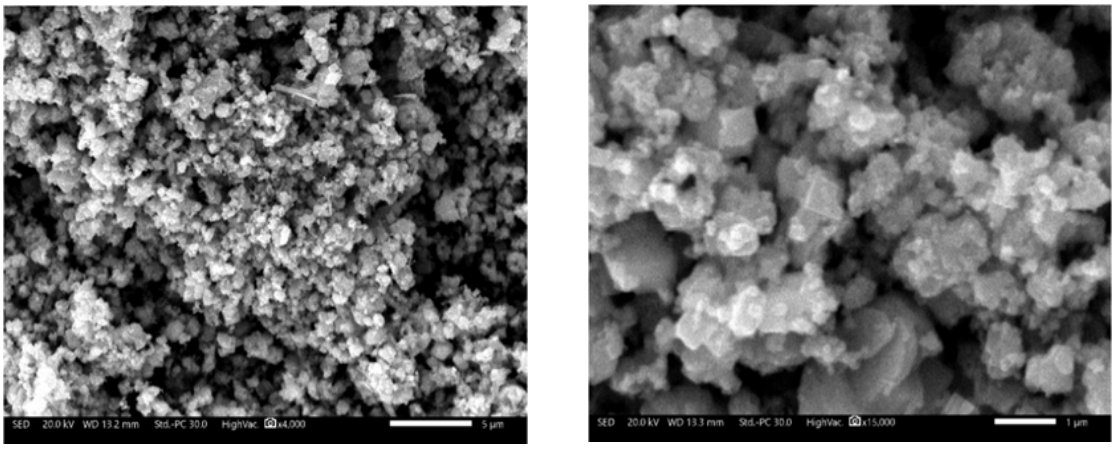

Fig. 4. SEM images of obtained $SrTiO_3$ at different magnifications.

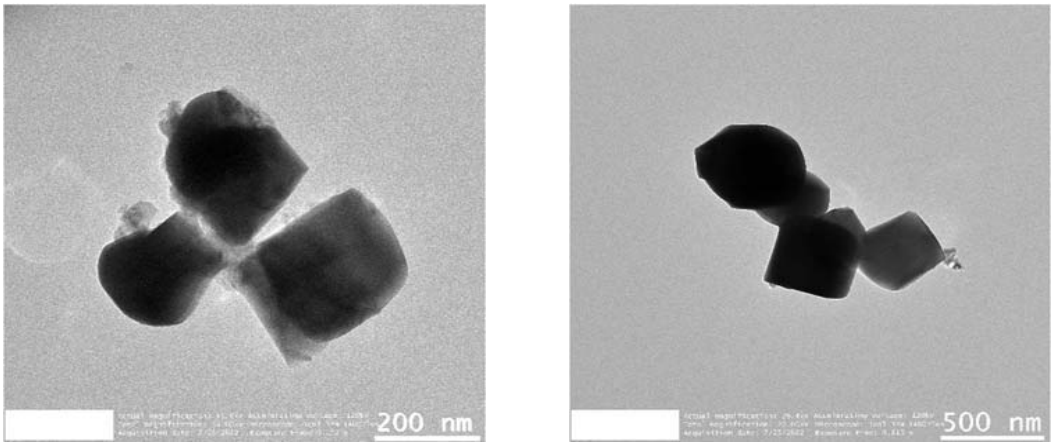

Fig. 5. SEM images of obtained $SrTiO_3$ at different magnifications.

The efficiency of solar energy conversion in semiconductor photocatalysts depends on the efficiency of charge separation. Without the presence of suitable active sites for photocatalytic reactions, photogenerated electrons and holes can easily recombine. It was found [38] that semiconductors such as TiO_2 and $BiVO_4$, which have characteristic anisotropic facets, can separate photogenerated electrons and holes into different facets. This separation provides selective reductive and oxidative reactivity on different facets. Mu et al. [38, 39] achieved the transformation of an isotropic 6-facet $SrTiO_3$ photocatalyst into an anisotropic 18-facet $SrTiO_3$ crystal and thereby significantly improved the separation of electrons and holes. They also found that the release of hydrogen and oxygen occurs at different crystal facets after the formation of an anisotropic $SrTiO_3$ facet. This strategy is the most promising way to increase photocatalytic activity since it allows to reduce charge recombination and reduces the need to search for various semiconductors necessary for the formation of a heterojunction.

3.2. DFT calculations

To investigate the electronic structure, the band structure and total density of states (TDOS) calculations were performed. The band structure shown in Fig. 6 (the Fermi energy is set equal to 0 eV on the ordinate axis) shows that the conduction zone minima lie at the Γ symmetry point, while the valence band maxima are at the R symmetry point. Thus, the indirect width of the bandgap (R-Γ) in the electronic structure for $SrTiO_3$ is 1.83 eV. There is an underestimation of the bandgap width compared to the experimental value of 3.20 eV, which is a typical problem for DFT-based calculations using the GGA-PBE method due to discontinuities present in the energy derivative of the number of electrons [17]. The value of the direct bandgap width (conduction band minima and valence band maxima at the Γ symmetry point) was 2.197 eV. The obtained results are in agreement with the data from other studies [40–43], but unlike them, in this work we did not carry out modeling of the $SrTiO_3$ supercell to minimize the

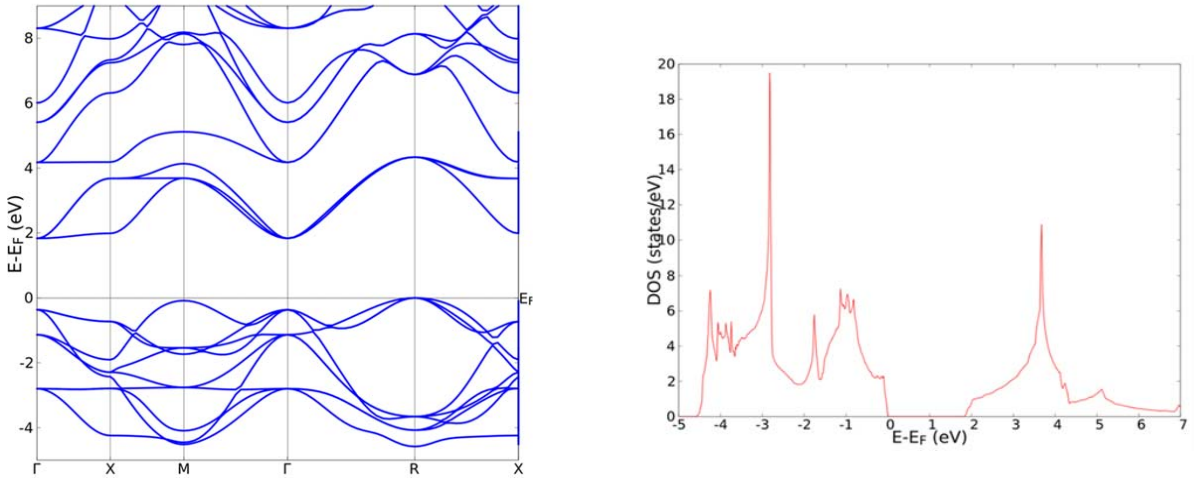

Fig. 6. Band structure and total density of states of $SrTiO_3$.

computational resources consumed and because we did not consider the doping of the crystal structure with impurity atoms.

It is well known that the band gap is a key factor that characterizes the electronic structure of materials and determines their application in electronics, so the accurate prediction of the band gap is a key issue in the development of new semiconductor materials. The PBE functional, which is very popular in DFT calculations due to its efficiency, due to the tendency to underestimate the band gap for semiconductor compounds and insulators, as has been demonstrated in many studies [17, 22, 43], as well as in this work, does not suitable for calculations of the electronic structure of semiconductor materials.

In order to achieve better accuracy in determining the width of the bandgap, some authors [24, 44] use hybrid functionals in calculations, such as PBE0, HSE, which provide better accuracy in calculating the lattice parameters of most solids and the bandgap width in semiconductors and insulators, give an excellent description of insulating antiferromagnetic oxides of rare-earth and transition metals [45]. For example, the paper [46] compares PBE, SCAN and HSE06 in DFT calculations for cesium antimonide and telluride and the authors conclude that SCAN is the best option for this type of materials, PBE is suitable for modeling structural parameters but should be avoided when quantitatively describing electronic properties, and HSE06 is excellent for determining electronic and optical gaps because it was designed for this purpose, but requires significant computational resources. Another approach to improve computational results is to introduce semiempirical terms into the GGA functional, such as GGA+U, in which the fitted Hubbard parameter U, is fitted to reproduce the experimental forbidden band width, geometry, and other parameters [25, 40, 45]. Therefore, it is worthwhile to further perform calculations relying on hybrid functionals to achieve the best fit to the experimental data.

To study the influence of doping on the structural and electronic properties of $SrTiO_3$, it is necessary to synthesize complex composites and perform DFT calculations. For this purpose, it is necessary to construct supercells with the introduction of impurity atoms, as was done in many works [1, 17, 24, 25, 41], as well as to calculate the optical properties of the materials.

4. Conclusion

$SrTiO_3$ was synthesized by a simple chemical precipitation method. X-ray diffraction data reveal the cubic structure of the synthesized $SrTiO_3$ and indicate the high crystallinity of the semiconductor. Elemental analysis was carried out using EDX analysis and FIB-SEM technique which showed the absence of impurities. A morphology study using SEM and TEM demonstrated the cubic structure of the formed particles of the obtained samples. The structural and electronic properties of $SrTiO_3$ were also investigated. The results were obtained using density functional theory in the framework of the GGA-PBE approximation. The band structure and density of states of $SrTiO_3$ demonstrate the presence of an indirect band gap, and the calculated parameters are suitable with the literature results.

Acknowledgments

This research is funded by the Science Committee of the Ministry of Science and Higher Education and of the Republic of Kazakhstan (No AP14869381).

References

[1]. A.C. Wardhana, A. Yamaguchi, S. Shoji, M. Liu, T. Fujita, T. Hitosugi, M. Miyauchi, *Appl. Catal. B: Environ.* 270 (2020) 118883. DOI: 10.1016/j.apcatb.2020.118883

[2]. T.K. Maji, Md.N. Hasan, S. Ghosh, D. Wulferding, C. Bhattacharya, P. Lemmens, D. Karmakar, S.K. Pal, *J. Photochem. Photobiol. A: Chem.* 397 (2020) 112575. DOI: 10.1016/j.jphotochem.2020.112575

[3]. Y. Liu, R. Li, H. Yang, J. Song, J. Hu, C. Yang, Z. Zheng, *Int. J. Hydrog. Energy* 47 (2022) 14563–14569. DOI: 10.1016/j.ijhydene.2022.02.207

[4]. P.K. Prajapati, A. Malik, N. Nandal, S. Pandita, R. Singh, S. Bhandari, S. Saran, S.L. Jain, *Appl. Surf. Sci.* 588 (2022) 152912. DOI: 10.1016/j.apsusc.2022.152912

[5]. J. Zhao, Z. Xiong, J. Wang, Y. Qiu, P. Liu, Y. Zhao, J. Zhang, *Chem. Eng. J.* 446 (2022) 137242. DOI: 10.1016/j.cej.2022.137242

[6]. J. Duan, X. Fang, C. Li, J. Qu, L. Guo, Y. Zou, M. Xiang, W. Wang, *Colloids Surf. Physicochem. Eng. Asp.* 659 (2023) 130759. DOI: 10.1016/j.colsurfa.2022.130759

[7]. K. Kato, T. Shirai, *J. Alloys Compd.* 901 (2022) 163434. DOI: 10.1016/j.jallcom.2021.163434

[8]. F.R. Sultanov, C. Daulbayev, B. Bakbolat, Z.A. Mansurov, *Eurasian J. Phys. Funct. Mater.* 2 (2018) 104–109. DOI: 10.29317/ejpfm.2018020202

[9]. F.R. Sultanov, Ch. Daulbayev, B. Bakbolat, Z.A. Mansurov, *Eurasian Chem.-Technol. J.* 20 (2018) 195-200. DOI: 10.18321/ectj721

[10]. H.K. Megbenu, Z. Tauanov, C. Daulbayev, S.G. Poulopoulos, A. Baimenov, *J. Chem. Technol. Biotechnol.* 97 (2022) 3375–3384. DOI: 10.1002/jctb.7197

[11]. A. Baimenov, F. Montagnaro, V.J. Inglezakis, M. Balsamo, *Ind. Eng. Chem. Res.* 61 (2022) 8204–8219. DOI: 10.1021/acs.iecr.2c00531

[12]. J.S. Gan, X.B. Li, U. Arif, F. Ali, A. Ali, F. Raziq, N. Ali, Y. Yang, Z. Wang, *Surf. Interfaces.* 39 (2023) 102938. DOI: 10.1016/j.surfin.2023.102938

[13]. M. Mousavi, J.B. Ghasemi, *J. Taiwan Inst. Chem. Eng.* 121 (2021) 168–183. DOI: 10.1016/j.jtice.2021.04.009

[14]. W. Navarra, I. Ritacco, O. Sacco, L. Caporaso, M. Farnesi Camellone, V. Venditto, V. Vaiano, *J. Phys. Chem. C* 126 (2022) 7000–7011. DOI: 10.1021/acs.jpcc.2c00152

[15]. D.I. Chenchik, J.M. Jandosov, *Eurasian Chem.-Technol. J.* 19 (2017) 191–195. DOI: 10.18321/ectj651

[16]. M.M.J. Sadiq, U.S. Shenoy, D.K. Bhat, *Front. Mater. Sci.* 12 (2018) 247–263. DOI: 10.1007/s11706-018-0433-0

[17]. H. Bantawal, U.S. Shenoy, D.K. Bhat, *Appl. Surf. Sci.* 513 (2020) 145858. DOI: 10.1016/j.apsusc.2020.145858

[18]. Y. Fo, M. Wang, Y. Ma, H. Dong, X. Zhou, *J. Solid State Chem.* 292 (2020) 121683. DOI: 10.1016/j.jssc.2020.121683

[19]. Z.A. Mansurov, *Eurasian Chem.-Technol. J.* 22(4) (2020) 241–253. DOI: 10.18321/ectj994

[20]. Y. Goto, T. Hisatomi, Q. Wang, T. Higashi, K. Ishikiriyama, T. Maeda, Y. Sakata, S. Okunaka, H. Tokudome, M. Katayama, S. Akiyama, H. Nishiyama, Y. Inoue, T. Takewaki, T. Setoyama, T. Minegishi, T. Takata, T. Yamada, K. Domen, *Joule* 2 (2018) 509–520. DOI: 10.1016/j.joule.2017.12.009

[21]. A.A. Aldongarov, A.M. Assilbekova, I.S. Irgibaeva, A.I. Mantel, *Eurasian J. Phys. Funct. Mater.* 4 (2020) 255–260. DOI: 10.29317/ejpfm.2020040308

[22]. R. Garcia-Diaz, M.T. Romero de la Cruz, R. Ochoa Valiente, J. Guerrero-Sanchez, G. Hernández Cocoletzi, *Appl. Surf. Sci.* 487 (2019) 1394–1402. DOI: 10.1016/j.apsusc.2019.05.134

[23]. H. Bentour, M. El Yadari, A. El Kenz, A. Benyoussef, *Solid State Commun*. 312 (2020) 113893. DOI: 10.1016/j.ssc.2020.113893

[24]. F. Opoku, K.K. Govender, C.G. Catharina Elizabeth van Sittert, P.P. Govender, *Int. J. Hydrog. Energy* 43 (2018) 22253–22264. DOI: 10.1016/j.ijhydene.2018.10.072

[25]. J. Wang, Y. Wang, Y. Wang, X. Zhang, Y. Fan, Y. Liu, Z. Yi, *Int. J. Hydrog. Energy* 46 (2021) 20492–20502. DOI: 10.1016/j.ijhydene.2021.03.147

[26]. F. Sultanov, C. Daulbayev, B. Bakbolat, O. Daulbayev, M. Bigaj, Z. Mansurov, K. Kuterbekov, K. Bekmyrza, *Chem. Phys. Lett*. 737 (2019) 136821. DOI: 10.1016/j.cplett.2019.136821

[27]. C. Daulbayev, F. Sultanov, A.V. Korobeinyk, M. Yeleuov, S. Azat, B. Bakbolat, A. Umirzakov, Z. Mansurov, *Appl. Surf. Sci.* 549 (2021) 149176. DOI: 10.1016/j.apsusc.2021.149176

[28]. F. Sultanov, C. Daulbayev, S. Azat, K. Kuterbekov, K. Bekmyrza, B. Bakbolat, M. Bigaj, Z. Mansurov, *Nanomaterials* 10 (2020) 1734. DOI: 10.3390/nano10091734

[29]. Z. Kuspanov, B. Bakbolat, A. Baimenov, A. Issadykov, M. Yeleuov, C. Daulbayev, *Sci. Total Environ.* 885 (2023) 163914. DOI: 10.1016/j.scitotenv.2023.163914

[30]. Z. Kuspanov, A. Umirzakov, A. Serik, A. Baimenov, M. Yeleuov, C. Daulbayev, *Int. J. Hydrog. Energy* (2023). DOI: 10.1016/j.ijhydene.2023.06.168

[31]. A. Habib, R. Haubner, N. Stelzer, *Mater. Sci.*

Eng. B. 152 (2008) 60–65. DOI: 10.1016/j.mseb.2008.06.018

[32]. B. Bakbolat, C. Daulbayev, F. Sultanov, R. Beissenov, A. Umirzakov, A. Mereke, A. Bekbaev, I. Chuprakov, *Nanomaterials* 10 (2020) 1790. DOI: 10.3390/nano10091790

[33]. P.K. Roy, J. Bera, *Mater. Res. Bull.* 40 (2005) 599–604. DOI: 10.1016/j.materresbull.2005.01.010

[34]. Y. Yang, B. Sun, G. Zhou, C. Ke, J. Zhang, Y. Zhou, S. Mao, J. Qin, Y. Zhao, *Mater. Today Commun.* 35 (2023) 105512. DOI: 10.1016/j.mtcomm.2023.105512

[35]. Z. Su, F. Fang, S. Liu, N. Wang, Y. Wan, D. Guo, W. Han and K. Chang, *Catal. Sci. Technol.* 12 (2022) 5003–5008. DOI: 10.1039/d2cy01146h

[36]. H. Nishiyama, T. Yamada, M. Nakabayashi, Y. Maehara, M. Yamaguchi, Y. Kuromiya, Y. Nagatsuma, H. Tokudome, S. Akiyama, T. Watanabe, R. Narushima, S. Okunaka, N. Shibata, T. Takata, T. Hisatomi, K. Domen, *Nature* 598 (2021) 304–307. DOI: 10.1038/s41586-021-03907-3

[37]. T. Takata, J. Jiang, Y. Sakata, M. Nakabayashi, N. Shibata, V. Nandal, K. Seki, T. Hisatomi, K. Domen, *Nature* 581 (2020) 411–414. DOI: 10.1038/s41586-020-2278-9

[38]. S.-C. Chan, Y.-L. Cheng, B.K. Chang, C.-W. Hong, *RSC Adv.* 11 (2021) 18500–18508. DOI: 10.1039/d1ra01711j

[39]. L. Mu, Y. Zhao, A. Li, S. Wang, Z. Wang, J. Yang, Y. Wang, T. Liu, R. Chen, Z. Jian, F. Fan, R. Li, C. Li, *Energy Env. Sci.* 9 (2016). DOI: 10.1039/C6EE00526H

[40]. A. Adewale, C. Abdullah, *Int. J. Nanoelectron. Mater.* 12 (2019) 11–18.

[41]. M. Rizwan, M. Anwar, Z. Usman, M. Shakil, S.S.A. Gillani, H.B. Jin, C.B. Cao, U. Mushtaq, *Chin. J. Phys.* 62 (2019) 388–394. DOI: 10.1016/j.cjph.2019.09.036

[42]. M. Rizwan, Z. Khadija, T. Mahmood, S.S.A. Gillani, M.I. Khan, *Phys. B Condens. Matter.* 602 (2021) 412553. DOI: 10.1016/j.physb.2020.412553

[43]. S.S.A. Gillani, R. Ahmad, Islah-u-din, M. Rizwan, M. Shakil, M. Rafique, G. Murtaza, H.B. Jin, *Optik* 201 (2020) 163481. DOI: 10.1016/j.ijleo.2019.163481

[44]. Y.S. Hou, S. Ardo, R.Q. Wu, *Phys. Rev. Mater.* 5 (2021) 065801. DOI: 10.1103/PhysRevMaterials.5.065801

[45]. J. Morin, J.M. Pelletier, Density Functional Theory: Principles, Applications and Analysis. Nova Science Publishers, Incorporated, New York, 2013, p. 3.

[46]. H.-D. Saßnick, C. Cocchi, *Electron. Struct.* 3 (2021) 027001. DOI: 10.1088/2516-1075/abfb08